Welding Parameters Optimization in Plunging and Dwelling Phase of FSW Medium Thickness 2219 Aluminum Alloy

Xiaohong Lu (lxhdlut@dlut.edu.cn)
Dalian University of Technology https://orcid.org/0000-0003-0520-3707
Jinhui Qiao
Dalian University of Technology
Junyu Qian
Dalian University of Technology
Shixuan Sun
Capital Aerospace Machinery Company
Steven Y. Liang
Georgia Institute of Technology

Research Article

Keywords: friction stir welding (FSW), medium thickness 2219 aluminum alloy, DEFROM, temperature distribution, optimization of welding parameters

Posted Date: December 3rd, 2021

DOI: https://doi.org/10.21203/rs.3.rs-1131926/v1

Version of Record: A version of this preprint was published at The International Journal of Advanced Manufacturing Technology on April 6th, 2022. See the published version at https://doi.org/10.1007/s00170-022-09098-z.

Abstract

The influence of welding parameters on temperature distribution in plunging and dwelling phase of friction stir welding (FSW) medium thickness 2219 aluminum alloy is blank. Improper selection of welding parameters will result in uneven temperature distribution along the thickness of the weldment, which will lead to welding defects and ultimately affect the mechanical properties of the weldment. To realize the prediction of temperature distribution and achieve the optimization of welding parameters, a simulation model of FSW 18mm thick 2219 aluminum alloy is built based on DEFORM. The validity of the simulation model is verified by temperature measurement experiments. With the minimum temperature difference in the core area of the weldment as target value, and weldable temperature range of 2219 aluminum alloy as constraint conditions, orthogonal experiments are conducted considering the rotational speed, the press amount, the tool tilt angle, the plunging traverse speed and the dwelling time. The results of variance analysis show that the rotational speed and the dwelling time are significant factors affecting temperature field during plunging and dwelling phase. Through single factor simulation, the welding parameters in plunging and dwelling phase are optimized. This study provides a reference for realizing high-quality welding of a heavy rocket fuel tank.

1 Introduction

A heavy-lift launch vehicle is the basic launch vehicle for the long-term development plans for spaceflight and deep space exploration. A rocket fuel tank is the main load-bearing structure of a rocket, which has extremely high requirements for manufacturing quality and reliability. The advanced rocket fuel tank is made of 2219 high-strength aluminum alloy with a thickness of 18mm. Friction stir welding (FSW) has the advantages of no need to add welding wire, no shielding gas, no pollution, no smoke, no radiation, high welding efficiency, small product deformation after welding, and excellent weld mechanical properties and has become the main connection process for the rocket fuel tanks [1].

The whole process of FSW includes three phases: plunging and dwelling, welding, and tool withdrawal phase. The plunging and dwelling phase is the initial phase, which will affect the subsequent welding phase. In this phase, the pin is slowly pressed into the weldment. The plasticization and flow behavior of the weldment material near the pin is the basis for the formation of the joint. Improper selection of welding parameters during plunging and dwelling phase of FSW 18mm thick 2219 aluminum alloy will result in high temperature gradient and uneven temperature distribution along the thickness of the weldment, and thus leads to defects in welded joints, such as flashes, holes, incomplete penetration, etc.. Welding defects directly affects the mechanical properties of the weldment. The thermo mechanical affect zone and weld nugget zone of the weldment are defined as the welding core area. The material flow in this area is intense, which directly affects the weld morphology and welding quality. It is difficult to measure the temperature distribution in the welding core area due to the tool rotation, shielding of the shoulder, material flow, and severe plastic deformation in the welding zone. Therefore, finite element method (FEM) has become an important means to study the temperature distribution in the welding core

area. At present, software such as ANSYS, MSC. Marc, FLUENT, ABAQUS and DEFORM are widely adopted to simulate the FSW process.

Scholars have simulated temperature distribution in the welding phase of FSW based on heat source model. McClure et al. [2], Jiang et al. [3] and Liu et al. [4] used the Rosenthal analytical method to analyze the transient temperature distribution in FSW process, and obtained the thermal cycle curve of each feature point in the welding zone. He et al. [5] and Wan et al. [6] used MSC. Marc established FSW simulation models, analyzed the ultrasonic-assisted FSW and FSW, and studied the temperature distribution during the welding process. Ren et al. [7] and Xu et al. [8] established FSW heat source model based on the torque heat source model, and used ANSYS to study the temperature distribution of the welding process and the residual stress after welding. Most scholars simulated FSW process based on heat source model, and studied the influence of welding parameters on temperature distribution. Complex nonlinear friction heat and plastic deformation heat in FSW process make it difficult to use analytical methods to describe temperature distribution.

Scholars have simulated temperature distribution in the welding phase of FSW based on FLUENT and ABAQUS. Eyvazian et al. [9] and Feng et al. [10] used FLUENT to simulate FSW process of dissimilar and same materials, and studied the temperature distribution of weldments. Yang et al. [11] used FLUENT to establish a simulation model for friction stir lap welding of dissimilar materials of Q235 steel and 6061 aluminum alloy, and studied the influence of different welding process parameters on the temperature distribution. Su et al. [12] and Yang et al. [13] established FSW simulation models of different stir pin shapes based on CFD method, and studied the effects of stir pin shape, shoulder radius, rotational speed and welding speed on temperature distribution in the welding process. The simulation method based on CFD has no strict restriction on the mesh size, but it cannot simulate the plunging and dwelling phase and the tool withdrawal phase, only the welding phase. Some scholars used ABAQUS to simulate FSW process, and studied the influence of size parameters of the tool and the welding parameters on temperature distribution of the weldment. Zhang et al. [14], Iordache et al. [15] and Liu et al. [16] used the Arbitrary Lagrangian-Euler (ALE) method in ABAQUS to avoid mesh loss, established FSW simulation model, and studied the velocity distribution, temperature distribution and equivalent plastic strain distribution during the welding phase, and studied the influence of different tool size parameters on the temperature distribution. ALE method usually ignores the simulation of plunging and dwelling phase to reduce the deformation of the mesh, and is difficult to simulate the whole process of FSW medium thickness weldment.

DEFORM attracted the attention of many scholars to simulate temperature distribution of FSW. Zhou et al. [17] and Han et al. [18] simulated the FSW process using local mesh refinement and adaptive following technology, obtained the temperature, strain distribution and material flow law of the welding process, and studied the influence of the rotational speed, welding speed and down pressure on the temperature distribution. Asadi et al. [19] used DEFORM to study FSW process of magnesium alloy, and adopted point tracking method to study the temperature distribution and material flow in the welding process. DEFORM has strong mesh refinement capability, which reduces the total number of meshes and

shortens the computation time. In the process of simulation, if the mesh deformation reaches a certain degree, DEFORM will automatically re-divide the global meshes to make the model easier to converge. Most notably, DEFORM can simulate the whole phase of FSW.

Scholars have carried out research on temperature distribution in the welding phase, and have drawn many meaningful conclusions. However, no research on the optimization of welding parameters in the plunging and dwelling phase has been done. There are many welding parameters in the plunging and dwelling phase, such as the rotational speed, the press amount, the tool tilt angle, the plunging traverse speed and the dwelling time. The influence law of the contributing factors on temperature are still blank. Different welding parameters are suitable for weldments of different materials and sizes. Therefore, it is necessary to study the influence of welding process parameters on the temperature field of FSW 18mm thick 2219 aluminum alloy during the plunging and dwelling phase, and to optimize the welding parameters. To realize the prediction of temperature distribution of FSW 18mm thick 2219 aluminum alloy and the optimization of the welding parameters, a simulation model of FSW is built based on DEFORM. The validity of the simulation results is verified by experiments. With the minimum temperature difference in the core area of the weldment as the target value, and the weldable temperature range of 2219 aluminum alloy as the constraint conditions, orthogonal experiments and variance analyses are carried out. The research determines the significant influence factors of the temperature difference and achieves the optimization of welding parameters in the plunging and dwelling phase.

2 Simulation Model Of Fsw Process Based On Deform

2.1 Geometrical Model and Meshing

The tool is composed of a shoulder with a concave angle and a conical stir pin, as shown in Fig. 1a. The radius of the shoulder is 16mm. The root radius and length of the conical stir pin are 7.5mm and 17.8mm, respectively. The weldment with the dimensions of 100 × 150 × 18mm^3 is modeled. The three-dimensional model after assembly is shown in Fig. 1b.

The mesh needs to be refined in the interaction area between the weldment and the tool to improve the simulation accuracy and coarsen on the outside of the interaction area to short the computation time. The position of mesh windows is shown in Fig. 2a. The size ratio is set to 4 to avoid the mesh outside the mesh windows from being too large to affect simulation accuracy. The mesh window density is set as 1 mm. The simulation model after meshing is shown in Fig. 2b.

2.2 Material Properties

The chemical composition of 2219 aluminum alloy is shown in Table 1. Fig. 3 gives the temperature-dependent material properties of the 2219 aluminum alloy.

Table 1
Chemical composition of 2219 aluminum alloy (wt%)

Cu	Mn	Fe	Si	Zn	V	Ti	Zr	Mg	Al
6.21	0.29	0.12	0.15	0.06	0.08	0.03	0.12	0.02	Bal

Define the weldment material type as visco-plastic material to reduce the chance of termination of the simulation [20, 21]. Johnson-Cook material model describes the effect of strain rate and temperature on flow stress and is used in FSW simulation [22]. Johnson-Cook constitutive equation is written as:

$$\sigma = \left(A + B\varepsilon^{n}\right)\left(1 + C\ln \dot{\varepsilon}^{*}\right)\left(1 - \left(T^{*}\right)^{m}\right) \quad (1)$$

$$T^{*} = \begin{cases} 0 & T < T_{room} \\ \left(\dfrac{T - T_{room}}{T_{melt} - T_{room}}\right) & T_{room} \le T \le T_{melt} \\ 1 & T > T_{melt} \end{cases} \quad (2)$$

Where ε presents the effective plastic strain; $\dot{\varepsilon}^{*}$ presents the relative plastic strain rate, $\dot{\varepsilon}^{*} = \dot{\varepsilon} / \dot{\varepsilon}_{0}$; $\dot{\varepsilon}$ presents the effective plastic strain rate; $\dot{\varepsilon}_{0}$ presents the reference plastic strain rate. The constants of the constitutive equation of 2219 aluminum alloy are shown in Table 2.

Table 2 Johnson-Cook constants of 2219 aluminum alloy [23]

A (MPa)	B (MPa)	n	C	m	T_r(℃)	T_m(℃)
170	228	0.31	0.028	2.75	15	590

2.3 Boundary Conditions and Frictional Model

Boundary conditions are divided into mechanical and thermal boundary conditions. Mechanical boundary conditions limit the degree of freedom of the weldment to ensure that the weldment is fixed during the simulation process. That is, limit the degree of freedom of movement in Z direction of the bottom surface of the weldment, and limit the degree of freedom of movement in X and Y directions of the side surface of the weldment.

Thermal boundary conditions setting mainly includes setting heat transfer mode and coefficient between the tool, weldment and backing plate. To shorten simulation time, heat convection coefficient of the bottom surface of the weldment and the air is used to simulate the heat conduction between the bottom surface of the weldment and the backing plate. Room temperature is set to 15°C, heat convection coefficient of the bottom surface of the weldment and the air is set to 5N/mm·s·°C, and heat convection

coefficient of the remaining surface of the weldment, the surface of the tool and the air is set to 0.025N/mm·s·°C [24].

During the welding process, the temperature of the contact area between the weldment and the tool increases, and the surface of the weldment material with lower strength is partially sheared. Under the action of friction, part of the weldment material will be stick to the surface of the tool. To describe the state of the contact area between the weldment and tool during the welding process accurately, shear friction model that changes with temperature is adopted. The equation is expressed as:

$$\tau = mk \qquad (3)$$

Where τ is the contact stress at the interface of the weldment and tool; m is the shear factor; k is the shear strength. The coefficients of friction are defined as temperature-dependent, as shown in Table 3.

Table 3
Temperature-dependent coefficients of friction [8]

Temperature (°C)	25	100	200	300	400	500
m	0.61	0.51	0.21	0.07	0.47	0

2.4 Implementation of simulation

Simulation of FSW 18mm thick 2219 aluminum alloy is realized, and the temperature distribution of the weldment in the three phases, i.e. plunging and dwelling, welding and tool withdrawal is obtained. The temperature distribution is shown in Fig. 4a, 4b, and 4c respectively.

3 Verification Of The Simulation Results

Temperature measurement experiments based on thermocouples are carried out in Capital Aerospace Machinery Company, and a temperature measurement system based on LabVIEW developed by our research group is used to collect the temperature data of the sampling points in the welding process. The thermocouples used for temperature measurement are K-type thermocouples, and the temperature measurement range is -200~1250°C. The FSW equipment is a large gantry FSW equipment, as shown in Fig. 5. The weldment with the thermocouples embedded is shown in Fig. 6.

The plunging traverse speed is 20mm/min, the welding speed is 100mm/min, the tool tilt angle is 2.5°, the press amount is 0.2mm, and the rotational speed is set as 350r/min, 400r/min, and 450r/min, respectively. Sampling points on the advancing side (AS) and the retreating side (RS) are obtained for temperature comparison to verify the validity of the built simulation model, as shown in Fig. 7.

Figure 8 shows the comparison of experimental and simulated temperature curves of sampling points on the AS and RS when the rotational speed is 400r/min.

The measured peak temperature on the AS and RS are 458.3°C and 429.9°C, respectively, and the peak temperature on the AS and RS obtained by simulation are 464.1°C and 434.5°C, respectively. The relative errors between the simulation and experimental peak temperature of the sampling points on the AS and RS are 1.27% and 1.07%, respectively.

Figure 9 shows the comparison of experimental and simulated temperature curves of feature points on the AS with rotational speed of 350r/min, 400r/min, and 450r/min.

From Fig. 9, we can see that the experiment and simulation feature point temperature change law is basically the same, and both have experienced the process of heating-peak-cooling. The measured peak temperatures on the AS are 413.2°C, 424.2°C, and 417.9°C, respectively, and the simulated peak temperatures on the AS are 426.1°C, 429.9°C, and 431.7°C, respectively. The relative errors of the simulation and experimental peak temperature on the AS are 3.12%, 1.34%, and 3.30%, respectively. The validity of the established simulation model is verified.

4 Optimization Of Welding Parameters In Plunging And Dwelling Phase

It has been proved that the friction heat generated by the friction between the shoulder and the weldment is higher than the friction heat generated by the stir pin [3, 4, 6]. In addition, the heat generated by the friction between the bottom surface of the tool and the weldment is transferred to the backing plate under the weldment, resulting in uneven heat input along the thickness of the weldment. The temperature difference in the core area of the weldment directly affects the joint structure, which ultimately affects the mechanical properties of the welded joint. Scholars have found that the part that hinders the overall tensile strength of the joint is the bottom joint of the core area [25–27]. If the bottom temperature increases, the dynamic recrystallization degree increases, the grain boundary angle increases, and the tensile strength of the joint increases. Therefore, the minimum temperature difference in the core area of the weldment is selected as the optimization goal.

When the temperature of the core area of the weldment is 80% of the melting temperature, the surface of the weld joint is smooth and the tensile strength of the joint is the highest [28]. The solidus temperature of 2219 aluminum alloy is 548℃, and the liquidus temperature is 649℃. 80% of the solidus and liquidus temperature are regarded as the upper and lower limits of the temperature in the core area of the weldment.

4.1 Influence of welding parameters on temperature difference of the weldment in plunging and dwelling phase

The welding parameters of the plunging and dwelling phase include the rotational speed, the press amount, the tool tilt angle, the plunging traverse speed and the dwelling time. All the welding parameters are selected as the factors of the orthogonal experiment, and the orthogonal experiment is carried out to

study the influence of the above parameters on the temperature difference of the weldment. The orthogonal table is shown in Table 4.

Table 4 Five factors and three levels of the orthogonal table

Level	Factor				
	Rotational speed (A)	Press amount (B)	Tool tilt angle (C)	Plunging traverse speed (D)	Dwelling time (E)
1	300r/min(A_1)	0.2mm(B_1)	1°(C_1)	20mm/min(D_1)	0s(E_1)
2	400r/min(A_2)	0.3mm(B_2)	2.5°(C_2)	40mm/min(D_2)	2.5s(E_2)
3	500r/min(A_3)	0.4mm(B_3)	4°(C_3)	60mm/min(D_3)	5s(E_3)

The sum of the freedom degrees of each factor is the number of factors × (number of levels - 1) = 5 × (3 - 1) = 10, which is less than the total freedom degree of $L_{18}(3^7)$. The orthogonal table is selected as $L_{18}(3^7)$.

The temperature difference between the peak and the minimum temperature in the core area is extracted through the post-processing module. The orthogonal experiment scheme and the temperature difference results are shown in Table 5.

Table 5 Orthogonal experimental results

Number	Factor					Temperature difference y_i (°C)
	Rotational speed (A)	Press amount (B)	Tool tilt angle (A)	Plunging traverse speed (B)	Dwelling time (C)	
1	1	1	1	1	1	187.63
2	1	2	2	2	2	138.84
3	1	3	3	3	3	117.34
4	2	1	1	2	2	116.55
5	2	2	2	3	3	102.92
6	2	3	3	1	1	151.22
7	3	1	2	1	3	65.08
8	3	2	3	2	1	130.89
9	3	3	1	3	2	98.08
10	1	1	3	3	2	159.56
11	1	2	1	1	3	114.74
12	1	3	2	2	1	221.86
13	2	1	2	3	1	159.47
14	2	2	3	1	2	112.03
15	2	3	1	2	3	95.15
16	3	1	3	2	3	74.20
17	3	2	1	3	1	135.17
18	3	3	2	1	2	85.85

The peak and minimum temperature in the core area of the 18 groups of models are shown in Fig. 10. Figure 10 shows that the peak temperature of the 18 groups of models does not exceed the upper limit of the temperature in the core area of the weldment. Only the minimum temperature of the 7th group model is within the weldable temperature range of 2219 aluminum alloy.

Then the mean square is calculated with the sum of squares and degrees of freedom to calculate the *F* test value. The analysis of variance table is shown in Table 6.

Table 6
Orthogonal experiment results

Source of variation	*SS*	*df*	*MS*	*F*	$F_{0.01}(2,7)$
Rotational speed (*A*)	10331.9	2	5165.95	35.77	9.55
Press amount (*B*)	113.68	2	56.84	0.39	
Tool tilt angle (*C*)	85.86	2	42.93	0.3	
Plunging traverse speed (*D*)	381.84	2	190.92	1.32	
Dwelling time (*E*)	14975.21	2	7487.61	51.85	
Error	1010.91	7	144.42		
Total variation	26899.4	17			

It shows that the rotational speed and dwelling time have a significant effect on the temperature difference of the weldment. Among them, the dwelling time has the greatest influence on the temperature difference, followed by the rotational speed.

4.2 Optimization of welding parameters in plunging and dwelling phase

The results of variance analysis show that the dwelling time and the rotational speed have significant influence on the temperature difference. Next, comprehensively research on the influence of the rotational speed and dwelling time on the temperature difference is conducted.

The plunging traverse speed is set as 20mm/min, the welding speed is set as 100mm/min, the tool tilt angle is set as 2.5°, the press amount is set as 0.2mm, the rotational speed is set as 300r/min, 400r/min, 500r/min, and 600r/min respectively, and the dwelling time is set as 0s, 2.5s, 5s, 7.5s, 10s, 12.5s, and 15s respectively. The peak temperature of weldment with different rotational speed and dwelling time is shown in Fig. 11.

Figure 11 shows a certain upward trend in the peak temperature during the dwelling phase of the different rotational speeds. When the rotational speed is 600r/min, the peak temperature exceeds the upper limit of the temperature in the core area of the weldment after dwelling for 2.5s. When the rotational speed is less than or equal to 500r/min, the peak temperature within 15s is lower than the upper limit of the temperature in the core area of the weldment.

The peak and the minimum temperature in the core area of weldment with different rotational speeds and dwelling times are shown in Fig. 12.

Figure 12 shows that when the rotational speeds at 300r/min and 400r/min, the minimum temperature in the core area of weldment is lower than the minimum value of the weldable temperature in the core area

of the weldment. When the rotational speed is 500r/min and the dwelling time is from 5s to 15s, the peak and the minimum temperature in the core area of weldment are both within the weldable temperature range of 2219 aluminum alloy. When the rotational speed is 600r/min, the peak temperature in the core area of weldment is higher than the maximum value of the weldable temperature in the core area of the weldment.

The temperature differences in the core area of the weldment with different rotational speeds and dwelling times are shown in Fig. 13.

Figure 13 shows that the higher the rotational speed, the smaller the temperature difference. There is no significant difference in the temperature difference when the dwelling time is in 5-15s range at the rotational speed of 500r/min and 600r/min. The reason may be that with the increase of rotational speed, the temperature of the contact area between the tool and the weldment increases, and the surface of the weldment material with lower strength is partially sheared. Under the action of friction, part of the weldment material will be stick to the surface of the tool, reducing the friction coefficient, which is manifested by the fact that there is no significant change in the temperature difference when the rotational speed increases to a certain extent.

When the dwelling time is 5s, the temperature difference of the weldment decreases sharply, and when the dwelling time is 15s, the temperature difference of the weldment decreases in significantly The reason may be that the tool and the weldment produce frictional heat during the FSW process after dwelling for 5s, and the plastic deformation heat generation and heat dissipation of the weldment reach a stable state.

From the above analyses, when the rotational speed is 500r/min, the dwelling time is 5s, the tool tilt angle is 2.5°, the plunging traverse speed is 20mm/min, and the press amount is 0.2mm, the temperature difference of the weldment is relatively small, so the optimal welding parameters for the plunging and dwelling phase is obtained.

5 Conclusion

To realize the effective prediction of temperature field of FSW medium thickness 2219 aluminum alloy and the optimization of the welding parameters, a simulation model of FSW 18mm thick 2219 aluminum alloy is established based on DEFORM, and the simulation of the plunging and dwelling, welding, and tool withdrawal phases is realized. The temperature field of weldment during the welding phase are obtained, and the effectiveness of the model is verified by experiment. The maximum relative error of the peak temperature of the sampling points is 3.30%, and the average relative error is 2.02%.

With the minimum temperature difference in the core area of the weldment as the target value, and the weldable temperature range of 2219 aluminum alloy as the constraint conditions, orthogonal experiments are carried out in consideration of the rotational speed, the press amount, the tool tilt angle, the plunging traverse speed and the dwelling time. The results of variance analysis show that the

rotational speed and dwelling time exert great influence on temperature field during the plunging and dwelling phase.

The simulation results show that when the rotational speed is 600r/min, the peak temperature exceeds the maximum value of the weldable temperature of 2219 aluminum alloy after dwelling for 2.5s. When the rotational speeds is 300r/min and 400r/min, the minimum temperature in the core area of weldment is lower than the minimum value of the weldable temperature of 2219 aluminum alloy. When the dwelling time is 5s, the temperature difference of the weldment decreases sharply, and when the dwelling time is further extended, there is no significant change in the temperature difference of the weldment.

Considering the processing efficiency and temperature difference comprehensively, the optimal welding parameters combination of FSW 18mm thick 2219 aluminum alloy in the plunging and dwelling phase is obtained: the rotational speed is 500r/min, the dwelling time is 5s, the tool tilt angle is 2.5°, the plunging traverse speed is 20mm/min, and the press amount is 0.2mm.

Declarations

Funding

The research was supported by the National Key Research and Development Program of China (Grant No. 2019YFA0709003), Dalian Science and Technology Innovation Fund (Grant No. 2020JJ26GX041) and the Fundamental Research Funds for the Central Universities (Grant No. DUT20ZD204). The financial contributions are gratefully acknowledged.

Conflicts of interest/Competing interests

Not applicable. The authors declare that they have no conflict of interest.

Availability of data and material

All data generated or analysed during this study are included in this manuscript.

Code availability

The code is available on request.

Authors' contributions

Xiaohong Lu: Conceptualization, Supervision, Methodology, Funding acquisition, Project administration.

Jinhui Qiao: Conceptualization, Methodology, Software, Validation, Writing - Original draft, Investigation, Writing - Review & Editing.

Junyu Qian: Formal analysis, Data curation.

Shixuan Sun: Software, Investigation, Formal analysis.

Steven Y. Liang: Resources.

Ethics approval

Not applicable

Consent to participate

Not applicable

Consent for publication

The authors consent that the work entitled as “Welding parameters optimization in plunging and dwelling phase of FSW medium thickness 2219 aluminum alloy” for possible publication in International Journal of Advanced Manufacturing Technology.

References

1. Chen GQ, Shi QY (2015) Recent Advances in Numerical Simulation of Material Flow Behavior during Frictions Stir Welding. J Mech Eng 51(22):11–21. https://doi.org/10.3901/JME.2015.22.011
2. McClure JC, Tang W, Murr LE, Guo X, Feng Z (1998) A Thermal Model of Friction Stir Welding. Trends Weld Res, Proc Int Conf 590-595
3. Jiang XD, Huang J, Zhou Q, Wang KH, Sun HY (2018) Numerical simulation of the temperature field for butt friction stir welding of dissimilar 6061-T6 and T2 alloys. Trans China Weld Inst 39(3):16–20. https://doi.org/10.12073/j.hjxb.2018390060
4. Liu WM, Yan YF, Sun T, Wu SY, Shen YF (2019) Influence of cooling water temperature on ME20M magnesium alloy submerged friction stir welding: a numerical and experimental study. Int J Adv Manuf Technol 105(12):5203–5215. https://doi.org/10.1007/s00170-019-04496-2
5. He DQ, Sun X, Zhu JM (2014) Numerical Simulation on Welding Temperature Field of 2024-T4 Aluminum Ultrasonic Assisted Friction Stir. Hot Work Technol 43(19):162–165. https://doi.org/10.14158/j.cnki.1001-3814.2014.19.044
6. Wan SQ, Wu YX, Gong H, Nie L (2019) Thermal Mechanical Coupling Simulation of Temperature and Residual Stress in Friction Stir Welding of 2219 Aluminum Alloy. Hot Work Technol 48(13):159–163. https://doi.org/10.14158/j.cnki.1001-3814.2019.13.042
7. Ren ZH, Li CX, Xie JX, Chen XJ (2018) Analysis on temperature field and residual stress field of ultrasonic friction stir welding. Trans China Weld Inst 39(11):53–57. https://doi.org/10.12073/j.hjxb.2018390272
8. Xu WF, Liu JH, Zhu HQ (2010) Numerical simulation of thermal field of friction stir welded 2219 aluminum alloy thick plate. Trans China Weld Inst 31(2):63–66

9. Eyvazian A, Hamouda A, Tarlochan F, Derazkola HA, Khodabakhshi F (2020) Simulation and experimental study of underwater dissimilar friction-stir welding between aluminium and steel. J Mater Res Technol 9(3):3767–3781. https://doi.org/10.1016/j.jmrt.2020.02.003
10. Feng YY, Zhao S, Liu ZS, Luo ZA (2021) Experiment Study and Simulation for Friction Stir Welding Process of 7075 Aluminum Alloy. J Northeast Univ Nat Sci 42(3):340–346. https://doi.org/10.12068/j.issn.1005-3026.2021.03.006
11. Yang JS, Liu HL, Huang CZ, Wang LM, Li JZ (2020) Numerical simulation of friction stir welding between steel and aluminum dissimilar metal based on Fluent. Weld Technol 49(8):11–15. https://doi.org/10.13846/j.cnki.cn12-1070/tg.2020.08.003
12. Su H, Wu CS (2021) Numerical Simulation for the Optimization of Polygonal Pin Profiles in Friction Stir Welding of Aluminum. Acta Metall Sin (Engl Lett) 34(8):1065–1078. https://doi.org/10.1007/s40195-021-01198-1
13. Yang ZY, Wang YL, Domblesky JP, Li WP, Han JM (2021) Development of a heat source model for friction stir welding tools considering probe geometry and tool/workpiece interface conditions. Int J Adv Manuf Technol 114:1787–1802. https://doi.org/10.1007/s00170-021-06985-9
14. Zhang Z, Chen JT, Wang JB, Wang H, Liu YL, Zhang HW (2011) Simulation Based Comparison of Friction Stir Welding of AA2024-T3 Plates with Different Thicknesses. J Mech Eng 47(18):23–27. https://doi.org/10.3901/JME.2011.18.023
15. Iordache M, Badulescu C, Niţu E, Iacomi D (2016) Numerical simulation of friction stir welding (FSW) process based on ABAQUS environment. Solid State Phenom 254:272–277. https://doi.org/10.4028/www.scientific.net/SSP.254.272
16. Liu CN, Yu ZK, Zhang YH, Niu XJ, Miao J (2018) Effect of pin shapes on temperature field in friction stir welding. Weld Technol 47(6):73–76. https://doi.org/10.13846/j.cnki.cn12-1070/tg.2018.06.021
17. Zhou MZ, Lei DG, Liang N, Yang JH (2010) 3D coupled thermo-mechanical visco-plastic finite element simulation of friction stir welding process. Trans China Weld Inst 31(2):5–9
18. Han R, Liu QP, Gao YH, Pan Y, Yang XH (2019) Fully coupled thermo-mechanical simulation analysis of friction stir welding for profile structure. J Plast Eng 26(4):293–299. https://doi.org/10.3969/j.issn.1007-2012.2019.04.043
19. Asadi P, Mahdavinejad RA, Tutunchilar S (2011) Simulation and experimental investigation of FSP of AZ91 magnesium alloy. Mater Sci Eng 528(21):6469–6477. https://doi.org/10.1016/j.msea.2011.05.035
20. Jain R, Pal SK, Singh SB (2016) A study on the variation of forces and temperature in a friction stir welding process: A finite element approach. J Manuf Proc 23:278–286. https://doi.org/10.1016/j.jmapro.2016.04.008
21. Nandan R, DebRoy T, Bhadeshia HKDH (2008) Recent advances in friction-stir welding - Process, weldment structure and properties. Prog Mater Sci 53(6):980–1023. https://doi.org/10.1016/j.pmatsci.2008.05.001

22. Al-Badour F, Merah N, Shuaib A, Bazoune A (2014) Thermo-mechanical finite element model of friction stir welding of dissimilar alloys. Int J Adv Manuf Technol 72(5-8):607–617. https://doi.org/10.1007/s00170-014-5680-3
23. Zhang ZQ, Jiang ZL, Wei QY (2017) Dynamic Mechanical Properties and Constitutive Equations of 2219 Aluminum Alloy. J Mater Eng 45(10):47–51. https://doi.org/10.11868/j.issn.1001-4381.2016.000859
24. Jain R, Pal SK, Singh SB (2019) Investigation on effect of pin shapes on temperature, material flow and forces during friction stir welding: A simulation study. Proc Inst Mech Eng Part B: J Eng Manuf 233(9):1980–1992. https://doi.org/10.1177/0954405418805615
25. Zhu R, Gong WB, Cui H (2020) Temperature evolution, microstructure, and properties of friction stir welded ultra-thick 6082 aluminum alloy joints. Int J Adv Manuf Technol 108(1-2):331–343. https://doi.org/10.1007/s00170-020-05422-7
26. Mao YQ, Ke LM, Liu FC, Chen YH, Li X (2016) Investigations on temperature distribution, microstructure evolution, and property variations along thickness in friction stir welded joints for thick AA7075-T6 plates. Int J Adv Manuf Technol 86(1-4):141–154. https://doi.org/10.1007/s00170-015-8182-z
27. Gao H, Dong JH, Zhang K, Luan GH (2014) Variations of the microstructure and mechanical properties for the thick aluminum friction stir welding joint along the thickness direction. Trans China Weld Inst 35(8):61–65
28. Ma ZS, Hou XY, Chen SR (2018) Effects of Sizes of Stirring Head Shoulder on Performance of 2219 Aluminum Alloy Friction Stir Welding Joint. Hot Work Technol 47(5):194–202. https://doi.org/10.14158/j.cnki.1001-3814.2018.05.050

Figures

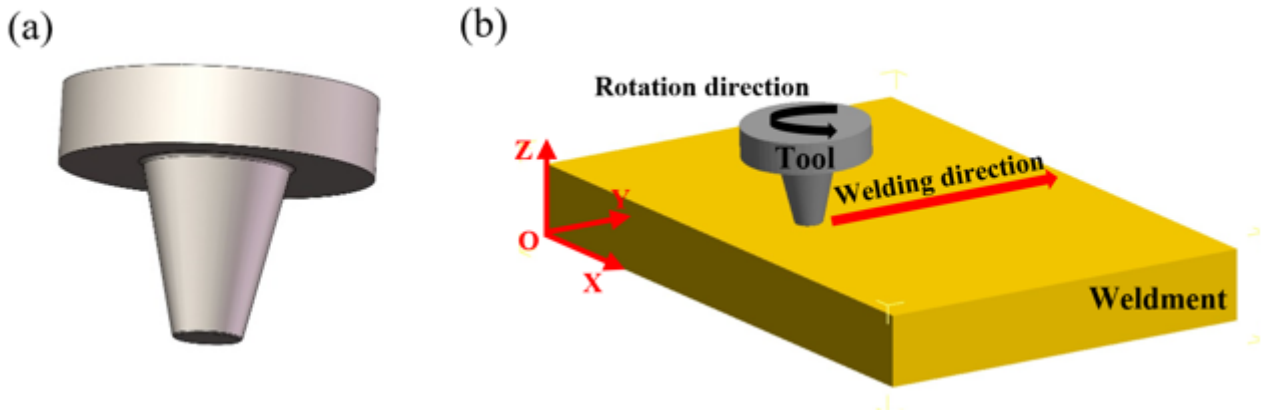

Figure 1

Geometrical model: a geometry of the tool, b three-dimensional model after assembly

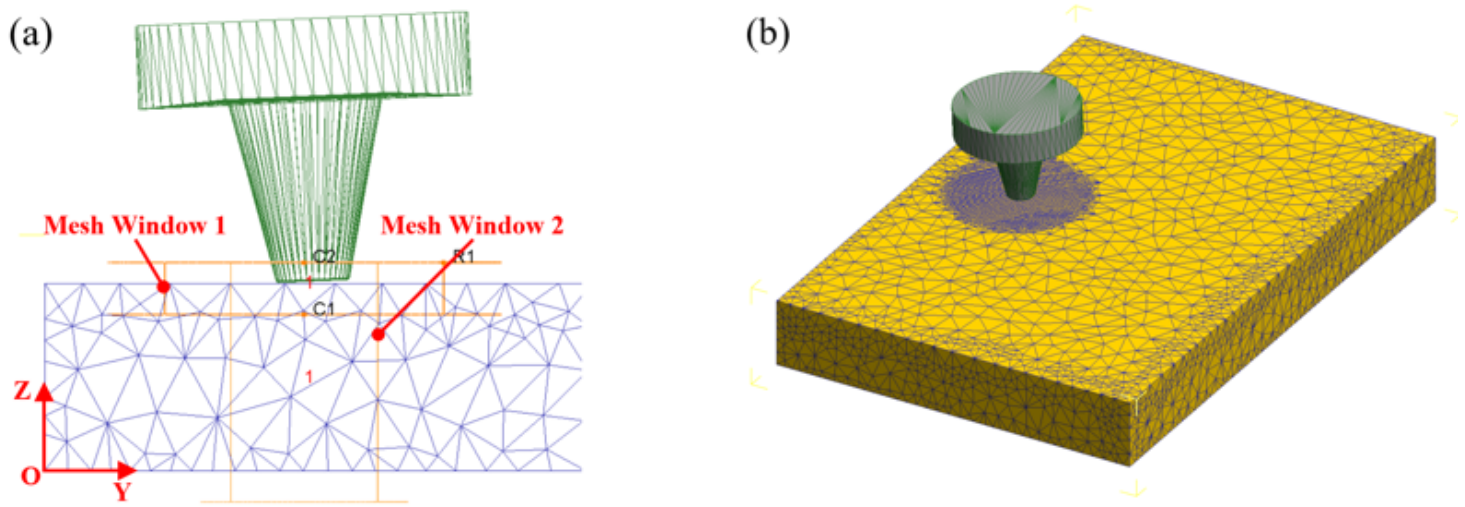

Figure 2

Meshing: a diagrammatic drawing of the mesh window position, b simulation model after meshing

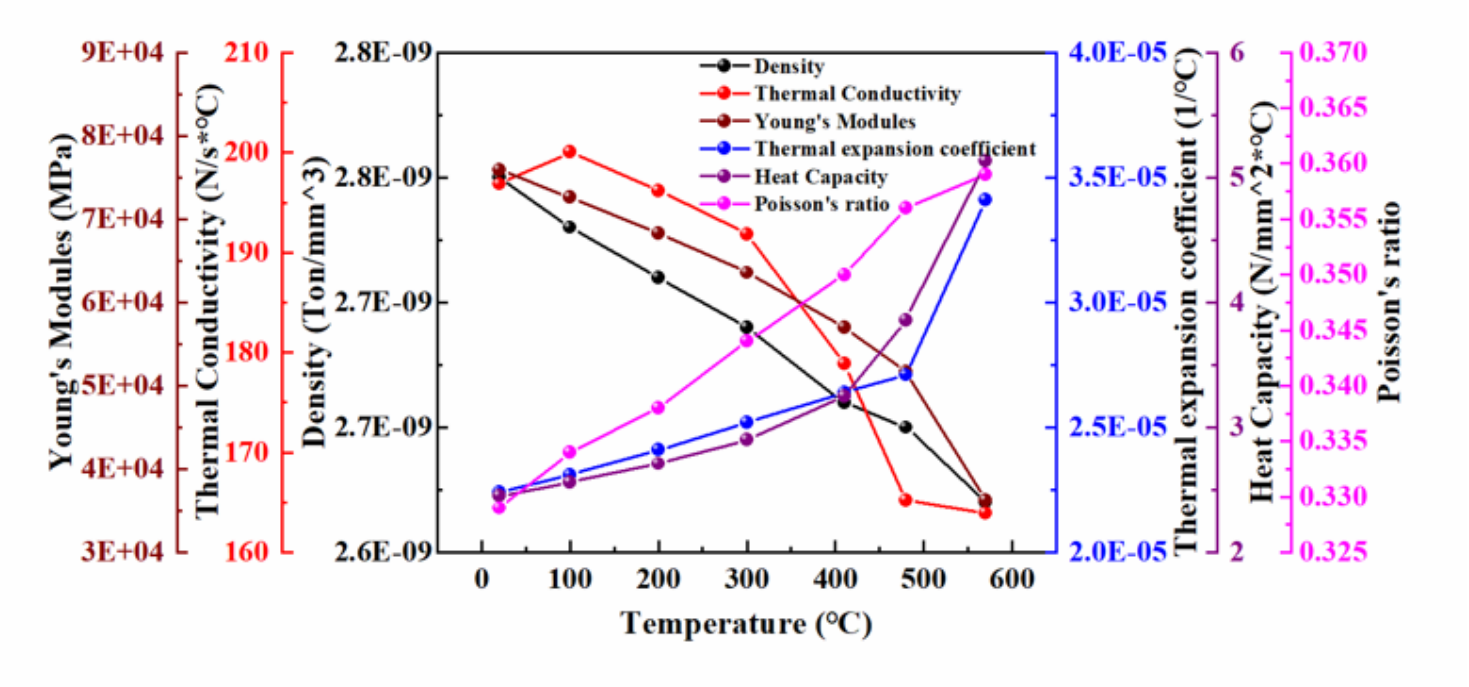

Figure 3

Temperature-dependent material properties of 2219 aluminum alloy

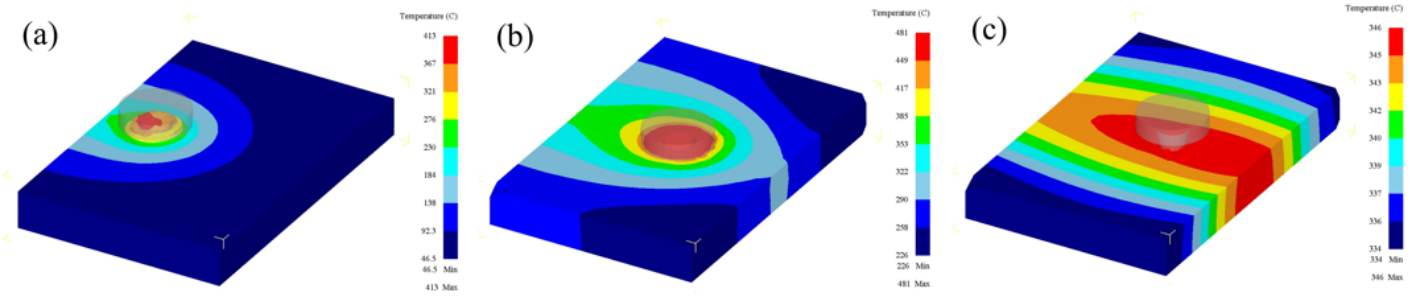

Figure 4

Temperature distribution: a the plunging and dwelling phase, b the welding phase, c the tool withdrawal phase

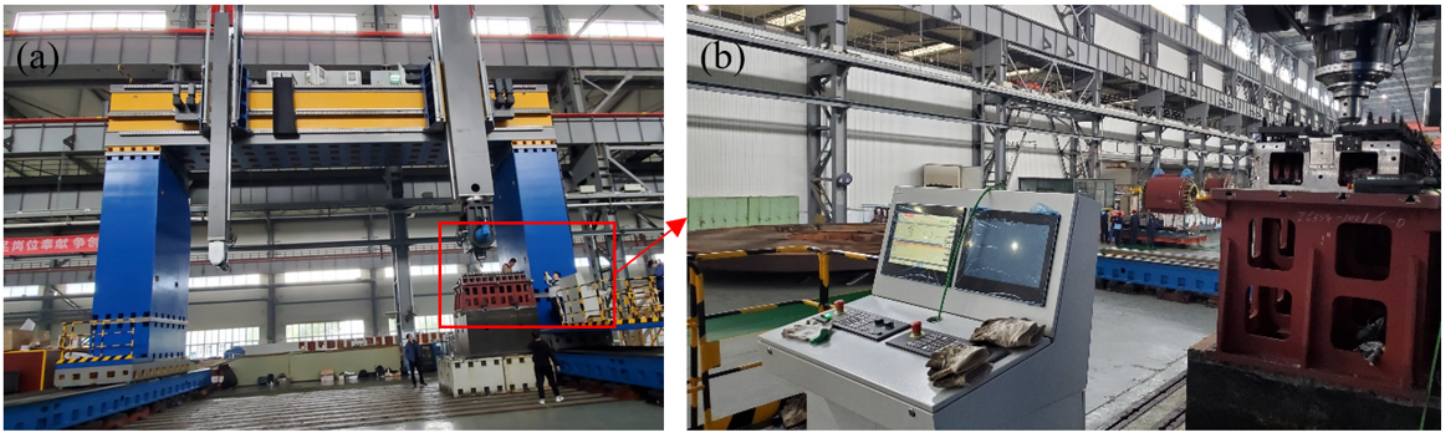

Figure 5

FSW equipment

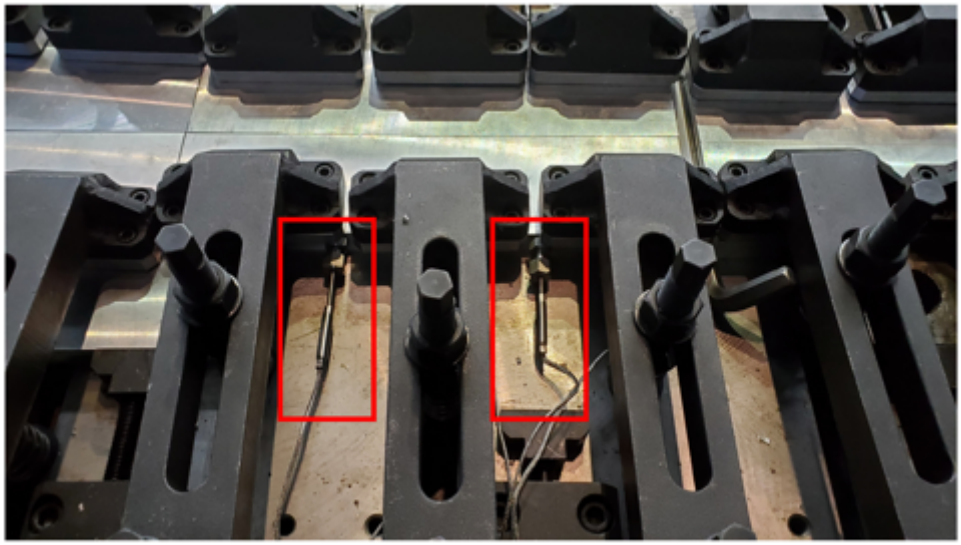

Figure 6

The weldment with the thermocouples embedded

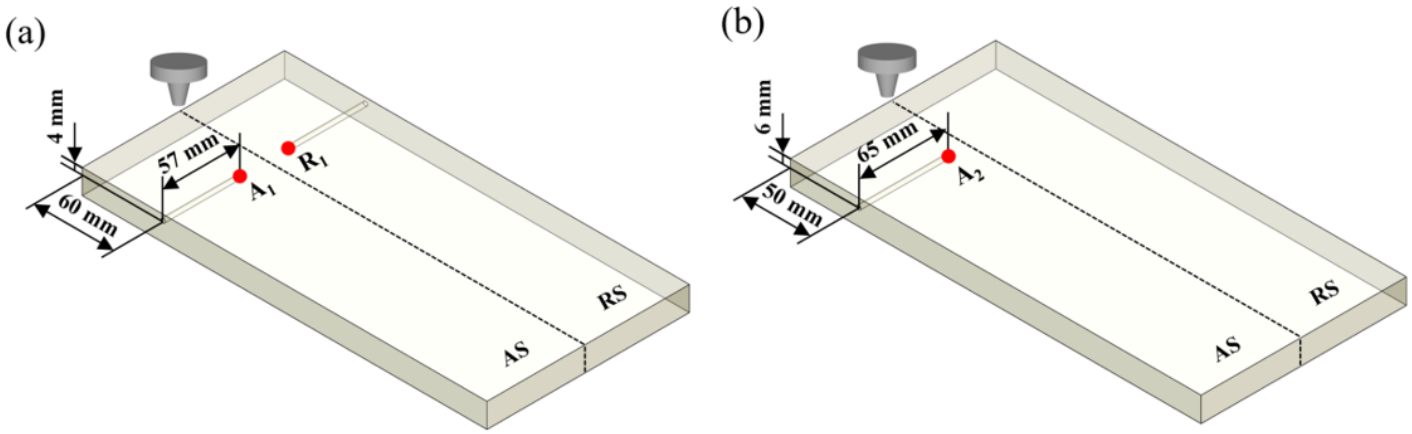

Figure 7

Schematic diagram: a feature points on the AS and RS, b feature points on the AS

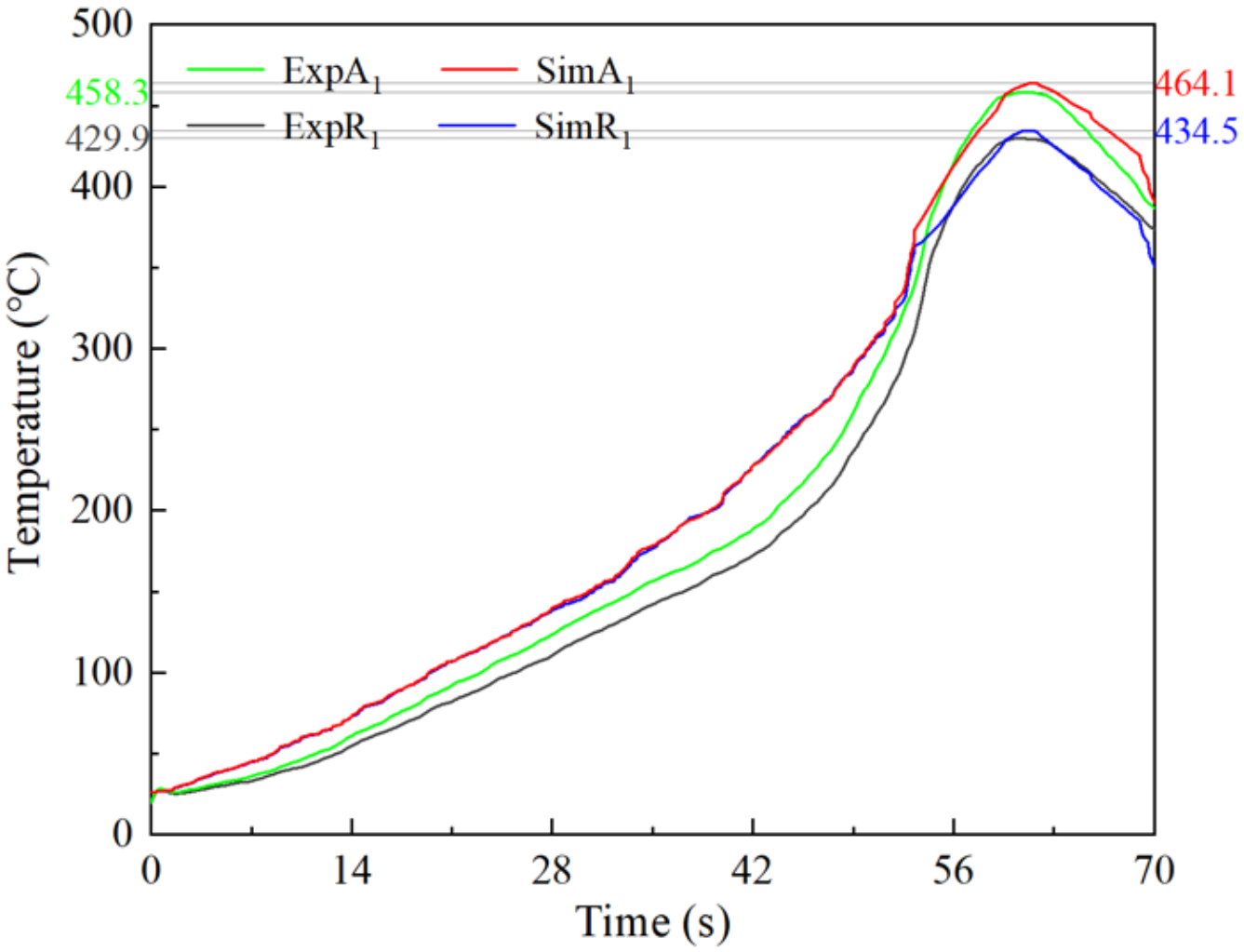

Figure 8

Comparison of experimental and simulated temperature curves of sampling points on the AS and RS

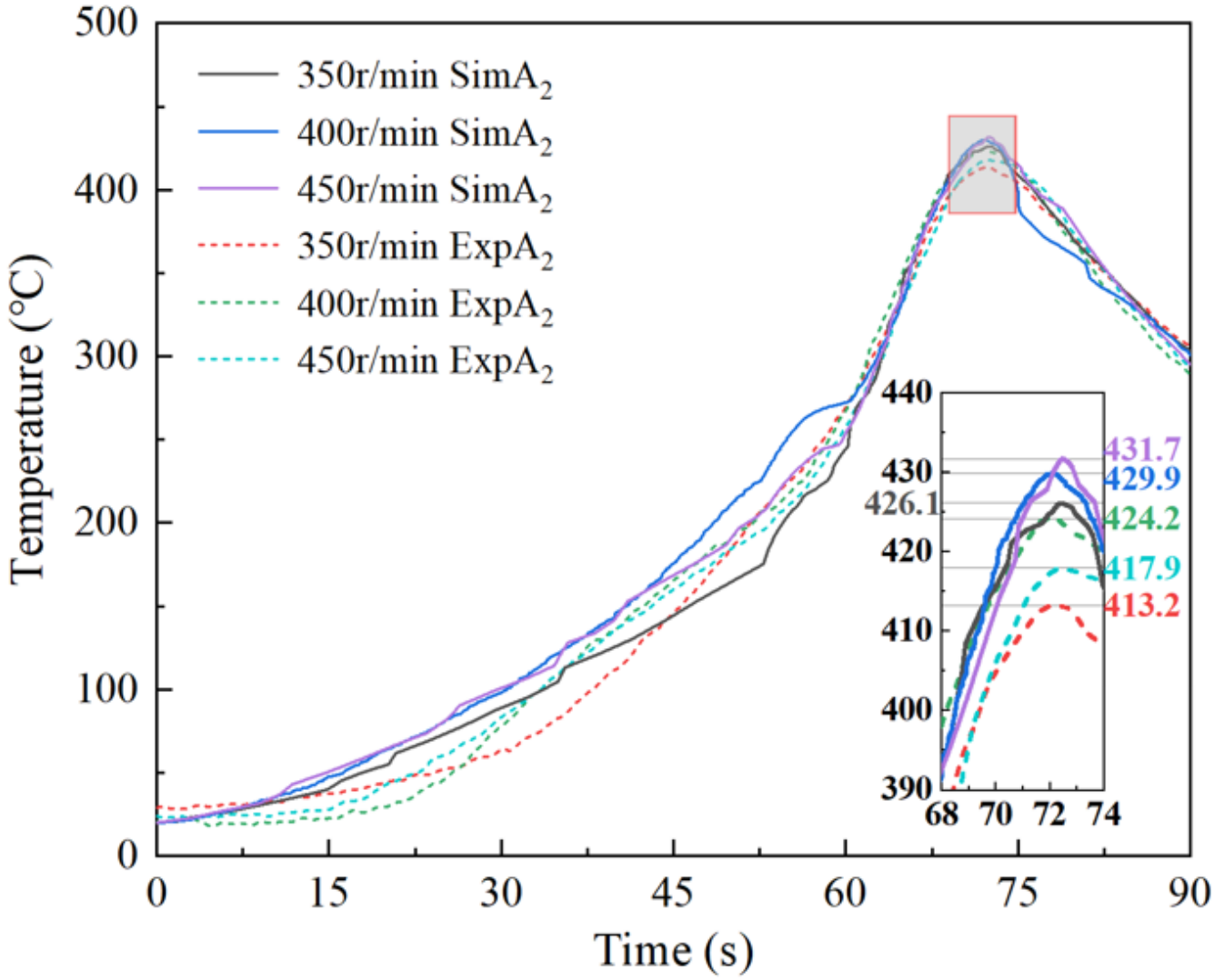

Figure 9

Comparison of experimental and simulated temperature curves of sampling points on the AS

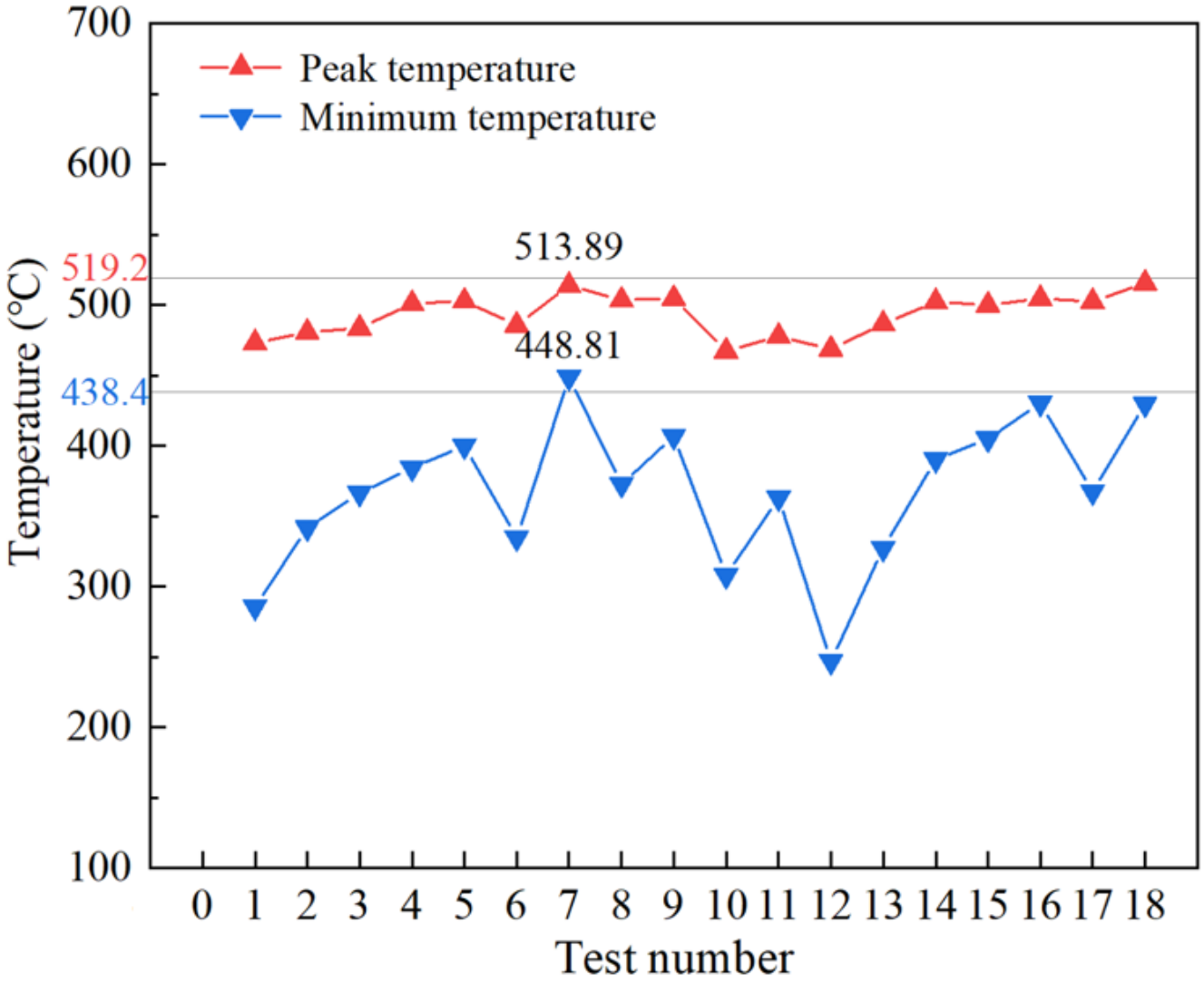

Figure 10

The peak and the minimum temperature in the core area of the weldment

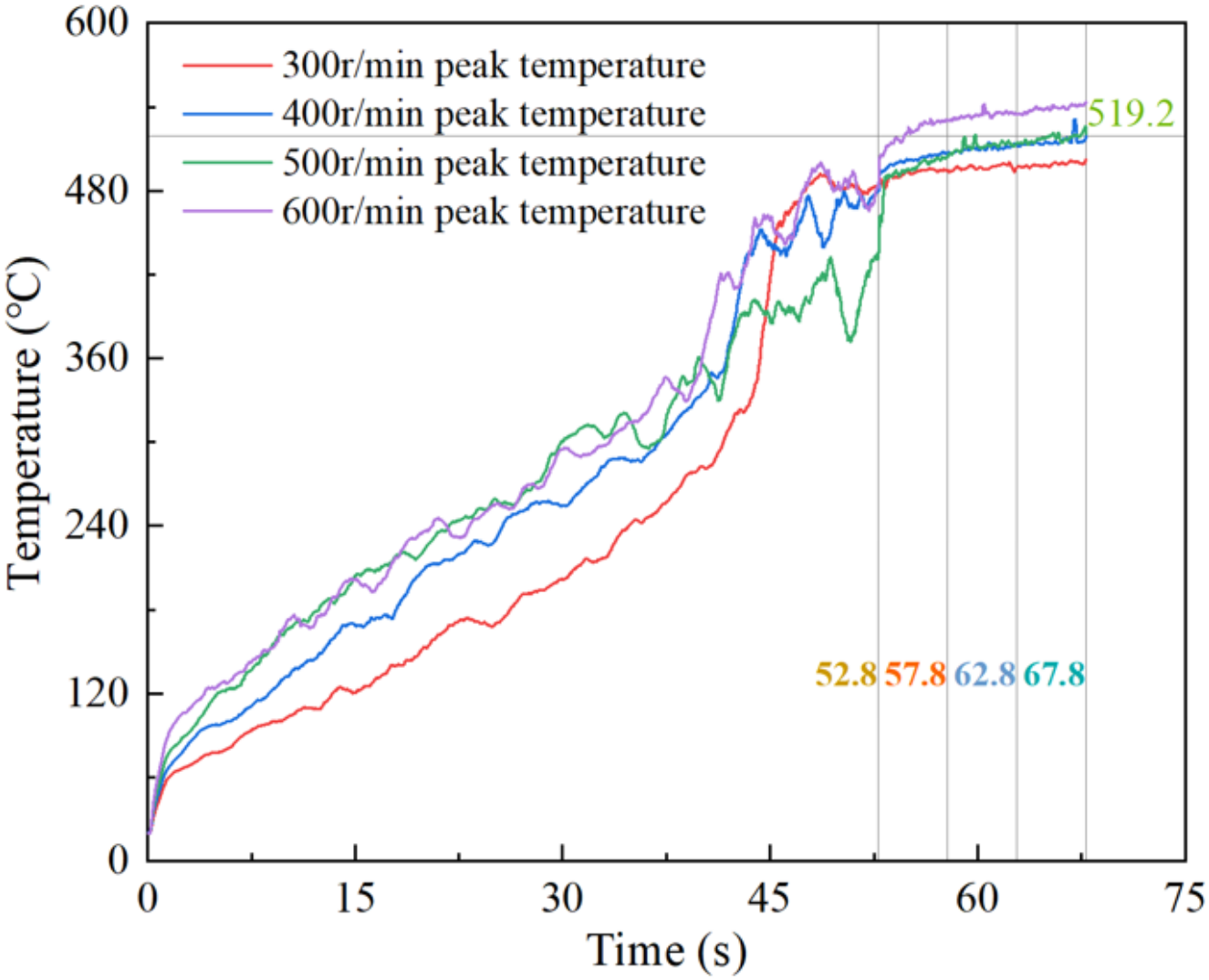

Figure 11

The peak temperature of weldment with different rotational speed and dwelling time

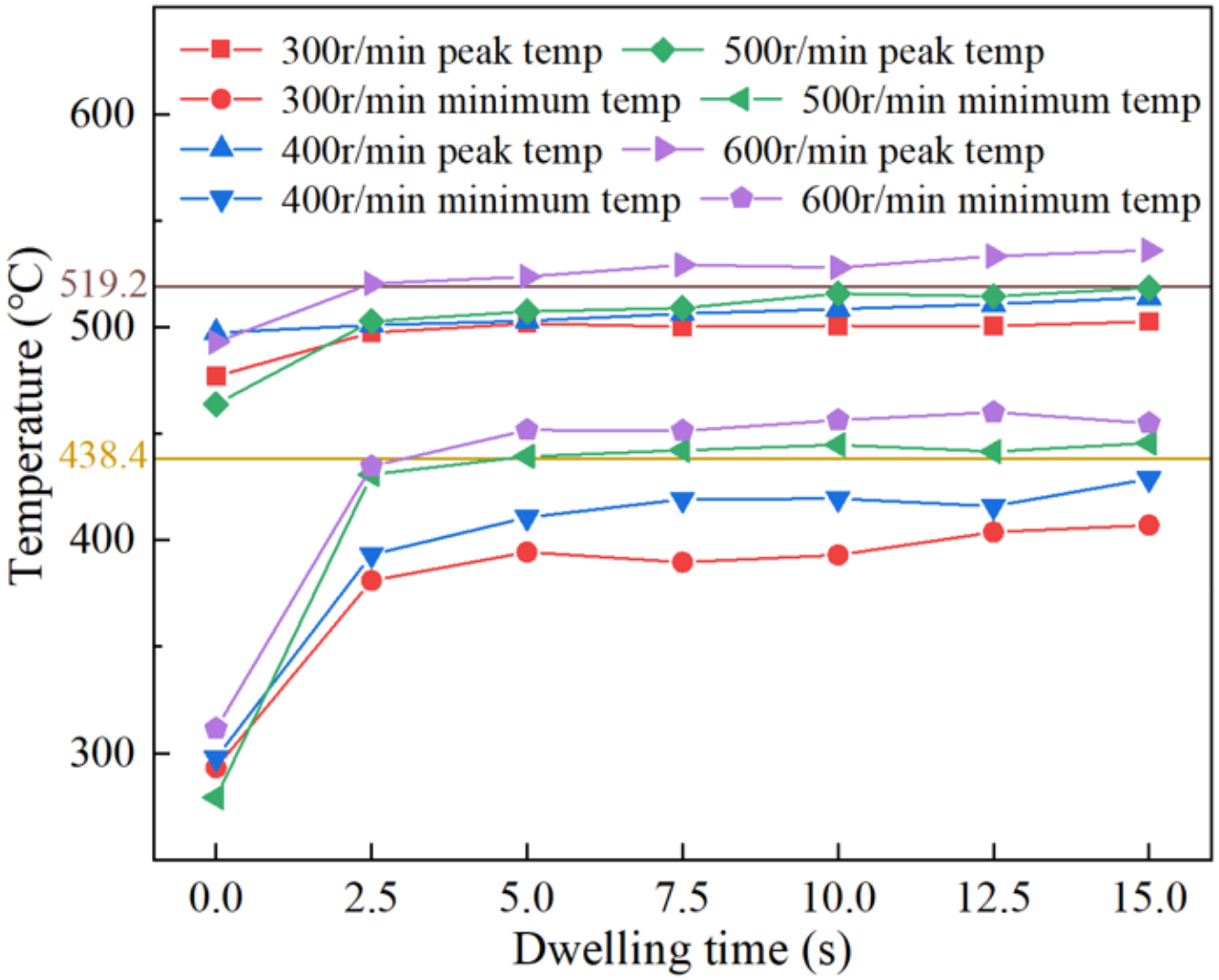

Figure 12

The peak and the minimum temperature in the core area of weldment with different rotational speeds and dwelling times

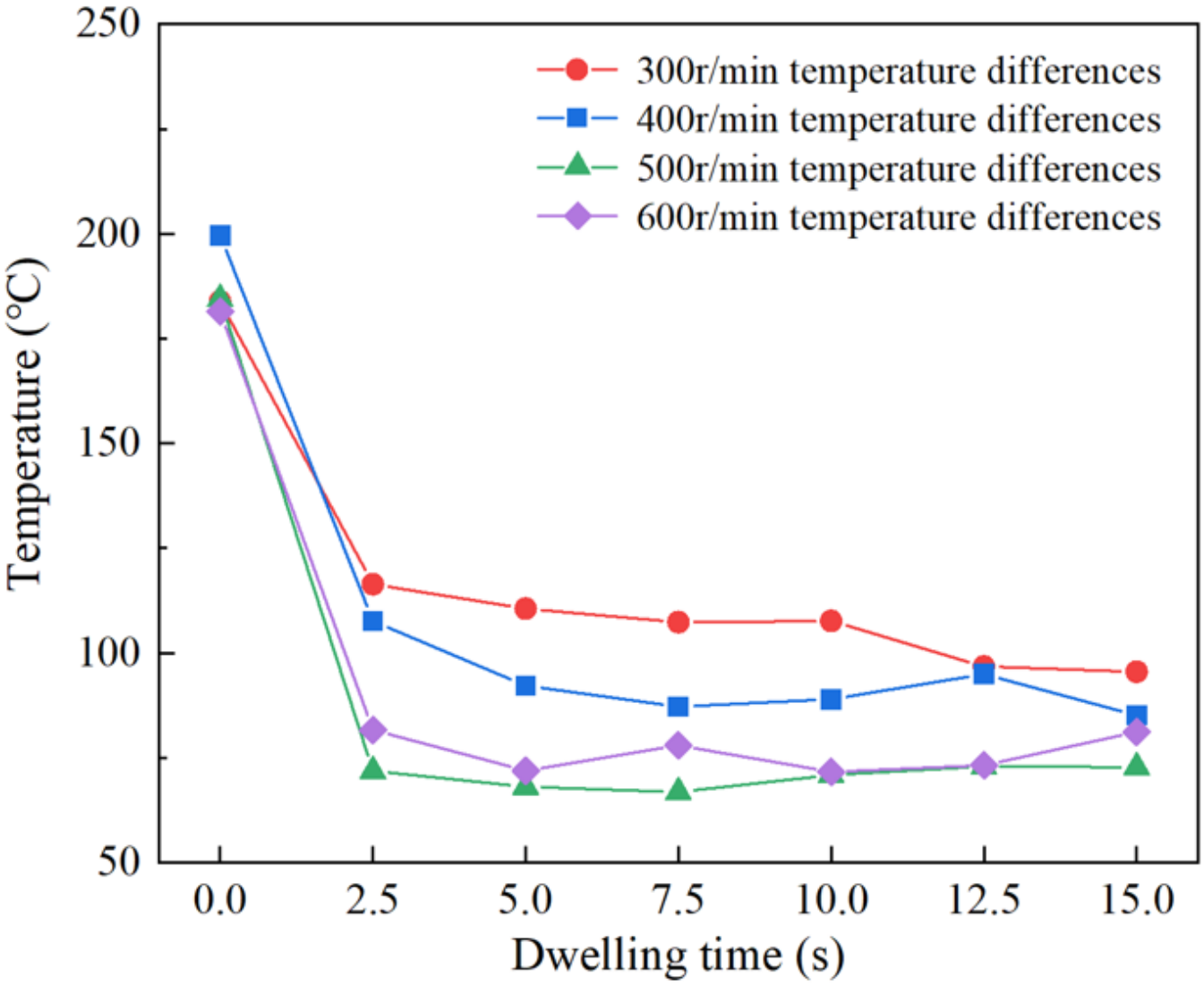

Figure 13

The temperature differences in the core area of the weldment with different rotational speeds and dwelling times